Available online at www.sciencedirect.com

ScienceDirect

Procedia Manufacturing 48 (2020) 485–491

Procedia MANUFACTURING

www.elsevier.com/locate/procedia

48th SME North American Manufacturing Research Conference, NAMRC 48 (Cancelled due to COVID-19)

Finish machining of Ti6Al4V SLM components under consideration of thin walls and support structure removal

Wolfgang Hintze, Robert von Wenserski*, Sebastian Junghans, Carsten Möller

Institute of Production Management and Technology, Hamburg University of Technology, w.hintze@tuhh.de

* Corresponding author. Tel.: +49 40 42878 3264; fax: +49 40 42731 4554. *E-mail address:* robert.von.wenserski@tuhh.de

Abstract

Using additive manufacturing (AM) technologies such as powder bed based selective laser melting, it is possible to realize new bionic designs for Ti6Al4V aerospace components, thus significantly reducing weight. With these technologies, the goals of reducing emissions in the aviation industry can be achieved while passenger numbers are growing at the same time. In order to fulfill the quality requirements of the components, the AM process chain includes many further process steps in addition to melting, such as heat treatment.
Furthermore, the functional surfaces must be machined and the support structures removed. These are essential for selective laser melting. The paper shows how the deflection of the workpiece can be minimized by milling thin-walled functional surfaces using a clamping device with support points. This increases the geometric accuracy considerably.
Finally, the paper shows the results for milling support structures. The design of the support structure has a high effect on the machining behavior. Finally, results are presented that show the influence of different milling strategies on the surface quality of AM components, considering the support structures.

Keywords: additive manufacturing, Support Structure, Precision Machining, SLM, Titanium, Milling

1. Introduction

According to forecasts on the long-term growth potential of the aviation industry, it can be assumed that 14,210 aircraft will have to be replaced and that an additional 25,000 aircraft will be needed within the next 20 years. This results in a demand of 39,210 new aircrafts. This high demand can be attributed to annual growth rates of 4.3% in the aviation sector [1].

Due to this growth and increasing environmental standards, various government aviation programs such as ACARE 2020 [2] or Flightpath 2050 [3] require significant savings in fuel consumption and reduction of emissions such as CO_2 or NO_x for the current aviation industry.

Achieving these goals requires the use of new technologies such as additive manufacturing (AM). AM can be used to bionically optimize the topology of aviation components, which reduces the weight of the components [4]. Here, numerical calculations are used to determine the part volume from a given design space that is of structural relevance [5]. In addition, complex assemblies can be combined to one component [6]. Powder bed based selective laser melting (SLM) is already an established AM technology for series production. Here, the material is melted layer by layer, so that the component is formed [7, 8].

Compared to laser metal deposition (LMD) components [9], SLM components have a higher dimensional accuracy and surface quality. Nevertheless, both components need machining for surfaces that require high accuracy. Fig. 1 shows further necessary process steps for SLM components. These are required to use the components in the aircraft. After SLM, heat treatment is usually carried out by stress relief annealing and hot isostatic pressing. This reduces thermal stresses and pores in the SLM components [10, 11, 12]. In addition, the AM semi-finished component has to be machined. Only then does the component surface fulfill the quality requirements of functional surfaces [13, 14, 15, 16]. Due to the low surface quality after

10.1016/j.promfg.2020.05.072

melting, the AM components also show a very low fatigue strength, which can be significantly increased by machining [11].

A challenge is the removal of support structures during post-processing. These are essential for selective laser melting. The supporting structures have the task of dissipating the heat. In addition, the support structures ensure geometric accuracy. Without support structures, the components would sink into the powder on overhanging geometries [17].

Another challenge is the machining of thin-walled structures. In order to keep the costs of selective laser melting low, AM components are usually designed with thin walls. These thin-walled components require special post-processing strategies in order to avoid bending [18, 19, 20] and distortion due to residual stresses [21] and thus ensure a high surface quality.

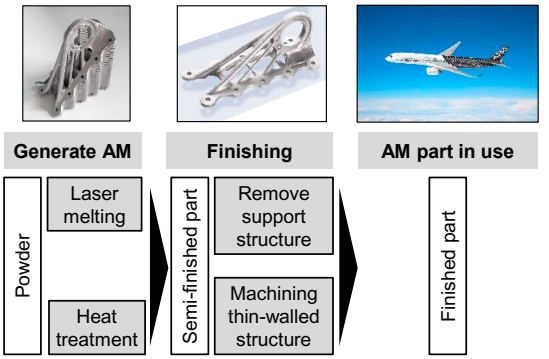

Figure 1 AM process chain [22, 23]

2. Milling thin-walled structures

Deviations occur on the workpiece surface during milling, because the workpiece deflects due to the cutting forces. Using an exemplary circumferential milling process, the following results show how deflection can be reduced during the machining of thin-walled AM components, like SLM workpieces, with a clamping device.

2.1. Process cycle of circumferential milling

Fig. 2 shows a typical process sequence for circumferential milling of a thin-walled SLM workpiece. The workpiece is machined with two infeeds (a_{p1}, a_{p2}). The two infeeds are necessary because often the cutting length l_2 is shorter than the milling surface. The test workpiece has a thin-walled, strongly overhanging (H) T-Geometry. This T-Geometry represents the conditions of thin-walled SLM series structural components in the aerospace industry.

In the first machining step, the upper surface of the workpiece is milled (I. 1st Machining step). Due to the machining strategy and the engagement conditions, the machining forces act on the workpiece with a very large lever arm. This results in a strong bending moment with deflection of the workpiece. After this first machining step, a strong form deviation of the surface becomes clear. Despite milling with a cylindrical tool, the surface shows an oblique shape deviation (II. Deflection). The further the workpiece overhangs, the more material remains unmachined. The reason for this is that the areas to be milled are pushed away in front of the cutting edge and therefore no machining of the material takes place.

Afterwards the milling is done with a second machining step (III. 2nd Machining step). Now the remaining lower machining surface is milled. The machining forces act on the workpiece with a low lever arm, so that a low bending moment with low deflection of the workpiece occurs. Due to the now very low workpiece deflection, the surface of the workpiece is milled with low roughness and low geometrical deviation.

However, as can be seen on the surface, a step is milled in the workpiece surface (IV. Surface deformation). The step is created due to the shorter cutting length l_2 of the tool compared to the height of the workpiece and is thus formed at the end of the cutting length. The step occurs in the area in which material was not milled in the first process step (I. 1st Machining Step) due to deflection. The height of the step is therefore a good indicator of the deflection of the workpiece during the post-processing of thin-walled structures.

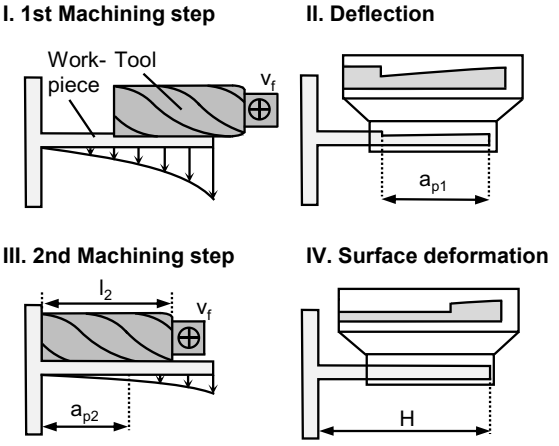

Figure 2 Process steps for finish milling thin-walled SLM components

2.2. Experimental methods, material and tool

The experimental setup used on the Heller MC12 machining center is shown in Fig. 3. A solid carbide end mill with number of teeth z = 4 and diameter d = 12 mm was used as milling tool. The end mill had a cutting length of l_2 = 24 mm. *Ti6Al4V* workpieces with a height H = 35 mm and a length L = 60 mm were used for milling. In the initial state, the workpieces had a thickness of t = 7 mm. As described in the process cycle, the surface was machined with two cutting depths $a_{p1} = a_{p2}$ = 16 mm and an engagement width a_e = 0.2 mm. After one machining cycle, the tactile measurement of the surface was carried out with the measuring device MahrSurf XR 20. The machining was then repeated so that the thickness of the workpiece was continuously reduced after each machining cycle. For measuring certainty, each test was repeated twice.

In comparison, a clamping device with high stiffness was used. The clamping device can be used to provide additional

support for the workpiece so that various clamping situations can be simulated. With the clamping device, only one side of the workpiece can be machined. To machine the other side, the workpiece must be turned over and re-clamped. For complete machining from both sides, the clamping device must be redesigned or another finishing strategy such as electrochemical polishing [24] is required. The occurring loads which cause a deflection at the workpiece were determined in previous milling tests. By analytical calculations of the bending line, a design of the clamping device could be identified. Especially overhanging workpiece geometries should be supported.

Furthermore, a Kistler 9257B dynamometer with which the process forces were measured was implemented in the setup. The raw signal was measured with the Kistler 5019B multi-channel charge amplifier. The sampling rate was 6 kHz using a low-pass filter of 2 kHz. The signal was then filtered with the smooth filter in MATLAB. Both signals are shown below.

The acceleration was measured with a triaxial accelerometer type PCB W356A03. The vibration of the workpiece was measured using a frequency of 51.2 kHz. The sensor was attached to the surface of the workpiece with wax on the back.

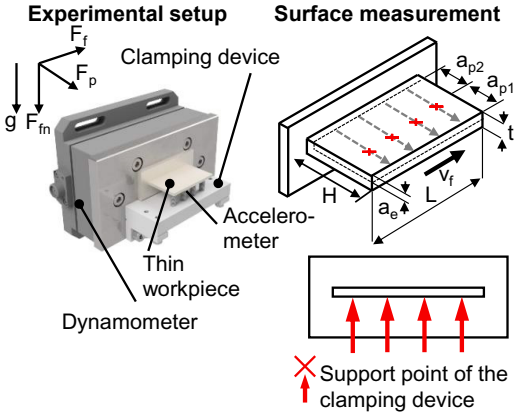

Figure 3 Experimental setup in the machining center for milling thin-walled structures

2.3. Results and discussion - Influence of the clamping device on the machining of thin workpieces

Fig. 4 shows the feed forces in the upper diagram and the shape of the workpiece surface in the lower diagram after several machining cycles for a final workpiece with a wall thickness of t = 2 mm. The final workpiece with a material thickness of t = 2 mm is very comparable to typical wall thicknesses of final structural SLM components which are used in airplanes. First, the results are displayed without additional support of the clamping device for the overhanging thin workpiece. The diagram with the process forces clearly shows the two machining areas along the processing time, which represent the two cutting depths a_p. The first force profile symbolizes the milling of the upper surface (a_{p1}) on the workpiece and the second force profile symbolizes the machining of the lower surface (a_{p2}).

When milling the upper surface (a_{p1}), the average feed force is $F_f = 61.1$ N and the average normal feed force is $F_{fn} = 106.1$ N. These values increase slightly when milling the lower surface. Now the average feed force is $F_f = 85.9$ N and the average feed normal force is $F_{fn} = 131.5$ N.

As already described for the process cycle, this is due to the fact that the workpiece is very strongly deformed during machining in the first process step. The material is not machined because it is pushed away in front of the cutting edge. When machining the lower surface, less deformation occurs due to the smaller overhang, so that more material is machined and a higher force level is achieved.

In addition, it is noticeable that the forces for both areas are not constant, they show a rising and falling trend. This suggests that the workpiece is also deformed at the start and end of milling. Especially at the beginning and at the end the workpiece is very unstable. In addition, the high vibration amplitude in the second process step is noticeable. This is due to a vibration of the workpiece due to the high overhanging length.

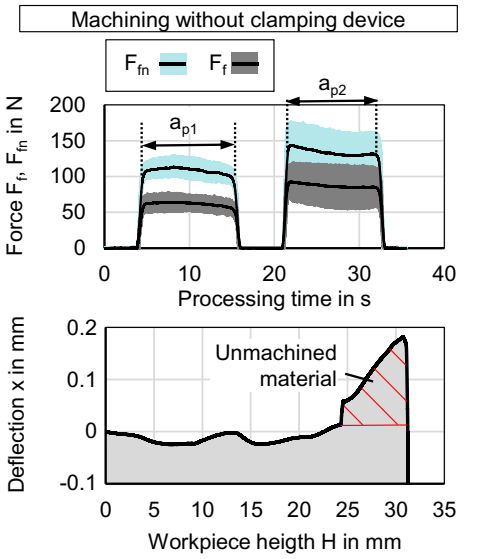

Process parameters				Tool
f_z	= 0.06 mm;	v_c	= 40 m/min	Solid carbide
a_e	= 0.2 mm;	a_{p1},a_{p2}	= 16 mm;	d = 12 mm
t	= 2 mm;	Emulsion 8 bar		z = 4
Process				No coating
Circumferential milling				

Figure 4 Machining behavior during machining without clamping device

The diagram below shows the surface after several process cycles with the final material wall thickness of t = 2 mm. The grey surface symbolizes the workpiece body in section and the black line indicates the workpiece contour. At a workpiece height H = 0 mm, the workpiece is firmly clamped to the dynamometer. At a workpiece height of H = 32 mm, the outer workpiece edge is presented. Due to the process cycle described in the previous chapter, with milling of the two machining surfaces in two cutting depths a_p, the step results in the height of x = 0.056 mm. In addition, the unmachined

material is clearly visible at high workpiece height, which was not machined due to the deflection of the workpiece.

Fig. 5 again shows the process forces for a workpiece with a wall thickness t = 2 mm in the upper diagram and the machined surface in the lower diagram. The workpiece was machined by milling over several cycles. Now, the results are displayed with additional support of the clamping device for the overhanging thin workpiece. The workpiece is supported at four points. The support points are located on the opposite workpiece surface of the milling operation. Once again, circumferential milling takes place in two cutting depths (a_{p1}, a_{p2}). First of all, it is noticeable that the force levels for both areas are very similar. From this it can be concluded that the milling behavior is very uniform and that the support prevents the workpiece from deflecting away.

In addition, the forces within a process step are very constant, so that no deformation of the workpiece occurs even at milling start and milling end. The noise of the forces is now also very low in the second process cycle (a_{p2}), so that a very low vibration of the workpiece due to the back support can be assumed. The good milling behavior resulting from the support also shows a very good surface with little deflection. The step resulting from the cutting length and the two cutting depths (a_{p1}, a_{p2}) at a workpiece height H = 24 mm has almost disappeared. Furthermore, it is clearly evident that even with a high workpiece height H only a very small form deviation occurs due to the deflection of the workpiece.

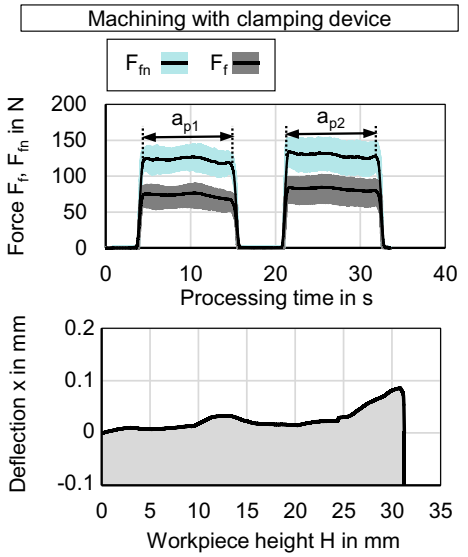

Process parameters				Tool
f_z	= 0.06 mm;	v_c	= 40 m/min	Solid carbide
a_e	= 0.2 mm;	a_{p1},a_{p2}	= 16 mm;	d = 12 mm
t	= 2 mm;	Emulsion 8 bar		z = 4
Process				No coating
Circumferential milling				

Figure 5 Influence of clamping device on forces and workpiece deflection

In-process measurement of workpiece displacement is challenging. For example, the use of laser triangulation sensors is difficult due to the use of emulsion. However, the influence of the clamping device on the vibration could be measured by using an accelerometer. In Fig. 6, the vibration signals with and without clamping device are directly compared. It can be seen that with support of the clamping device, the amplitude of the acceleration is much higher than without clamping device. As a result, the support of the clamping device has significantly reduced vibrations.

It can be concluded that suitable clamping systems for SLM workpieces can significantly improve the milling behavior and thus the geometric accuracy of thin-walled workpieces.

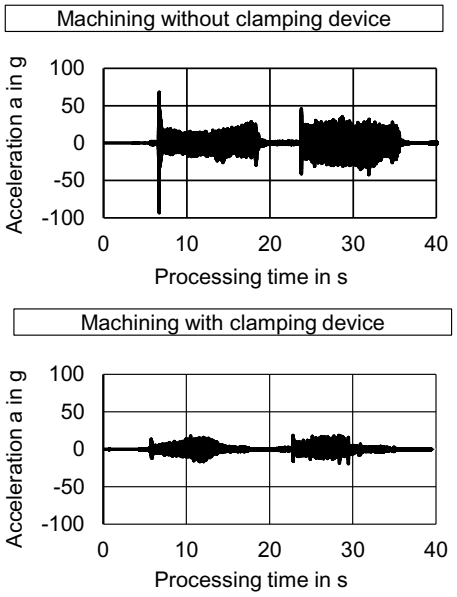

Process parameters				Tool
f_z	= 0.06 mm;	v_c	= 40 m/min	Solid carbide
a_e	= 0.2 mm;	a_{p1},a_{p2}	= 16 mm;	d = 12 mm
t	= 2 mm;	Emulsion 8 bar		z = 4
Process				No coating
Circumferential milling				

Figure 6 Influence of the clamping device on vibration

3. Milling of support structures

According to the current state of the art, the support structures are usually removed manually. For series production of SLM components, automated removal of the support structures is essential. One approach is milling the support structures, comparable to rough milling. So far, many force models exist for the machining of solid material [25, 26]. However, there is little knowledge about the influence of different support structure designs on the milling process.

3.1. Support structure geometries

Fig. 7 shows various geometries. These are typical *Ti6Al4V* support structure geometries. In addition, the supporting structures are shown schematically in cross-section. The support structure of type A is a hollow geometry composed of square columns which are perforated. The geometry of support

structure type B are bent, solid columns. The type C support structure is a solid support structure used to create strong support on critical overhangs. In addition, support structure type C has a wavy geometry in xy-direction to further increase the stiffness.

For comparability, the material volume fractions of the support structures are taken into account. The machining by circumferential milling is carried out with a cutting depth of $a_p = 8$ mm. Fig. 7 shows the cross-section of the support structure which is proportional to this cutting depth and which is in contact with the tool. With regard to the cutting depth, type A and type B have the same very low material volume fraction. Type C has a high material volume fraction for a support structure due to the high thickness of the support structure without perforation.

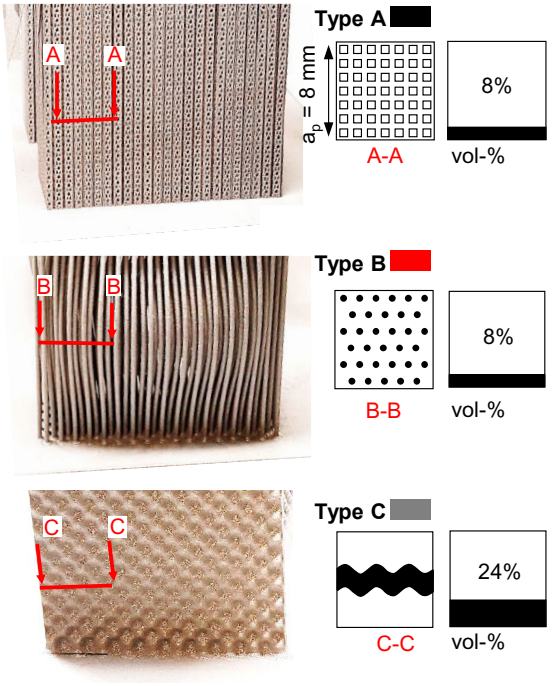

Figure 7 Geometry of the support structure with the corresponding material volume fraction related to the cutting depth a_p

3.2. Experimental methods, material and tool

The experimental setup is shown in Fig 8. The support structure was milled by circumferential milling with a cutting depth of $a_p = 8$ mm. For support structure type C, the cutting depth corresponded to the thickness of the support structure ($a_p = 2$ mm).

A solid carbide tool with number of teeth z = 4 and diameter d = 8 mm was used. Due to the geometry of the support structure, a variable engagement width a_e is assumed, because there is a discontinuous contact to the support structure at the circumference of the tool [14].

During milling, the forces were measured using a dynamometer. Once again, the measurement was carried out using a Kistler 5019B multi-channel charge amplifier with a sampling rate of 6 kHz and a low-pass filter of 2 kHz. The feed rate and therefore the feed force was in the direction of the x-force of the dynamometer. In addition, each test was repeated three times.

The MahrSurf XR20 device was used to measure roughness. The measurement was carried out with a tactile sensor, which had a radius of 2 µm and a tip made of diamond. For each surface, 10 roughness measurements were carried out and the evaluation was done in accordance to ISO 4287.

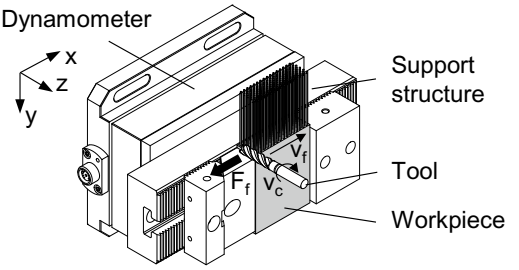

Figure 8 Experimental setup in the machine center Heller MC12 for milling support structures

3.3. Results and discussion - Influence of the support structure geometry on the milling forces and influence of the milling strategy on the surface quality

The feed forces which occur during circumferential milling of the various support structures are shown in Fig. 9. First, it is noticeable that the mean level of forces for type A and type B are significantly lower than the forces for type C. This is the result of the different material volume fractions. Because of the higher material volume fraction in type C, the metal removal rate is higher, resulting in the higher average force level. Furthermore, it is noticeable that the forces of type A and type B oscillate very strongly. This is caused by the geometry.

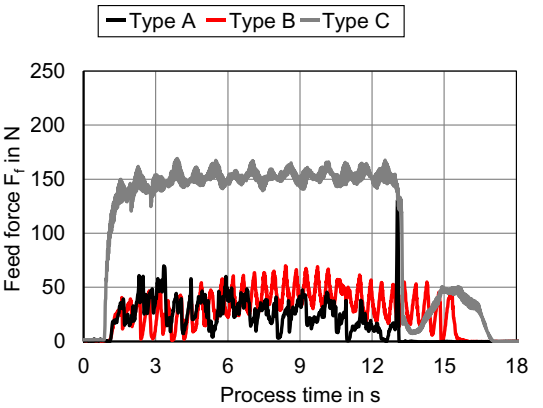

Process parameters
v_c = 50 m/min; f_z = 0.06 mm/z
a_p = t_{supp} = 2 - 8 mm; a_e = variable
Internal cooling

Process
Circumferential milling

Tool
Solid carbid; z = 4
No coating; d = 8 mm

Figure 9 Influence of different support structure geometries on the feed force during milling

Every time the cutting edge comes into contact with a new support structure element, a new peak is created in the force curve. Fluctuations of force can also be seen in the curve of the type C support structure. These are presumably caused by the wavy geometry of the support structure.

In order to reduce the process times during post-processing, a current research approach is to remove the support structure and simultaneously finish the functional surface. This strategy (Surface machining 1 Step) is shown in Fig. 10. As an alternative, the supporting structure can first be removed by rough milling and then the SLM surface can be machined by finish milling (Surface machining 2 Steps). For these two machining strategies, the surface roughness was measured after milling and compared with the surface roughness of the SLM surface. It is noticeable that surface roughness can be strongly reduced by machining and that quality requirements of functional surfaces are only fulfilled after milling.

In addition, it can be seen that machining in 2 steps doubles the process time, but the surface roughness is again significantly reduced compared to simultaneous milling. This is the result of the discontinuous contact between tool and support structure when machining support structure and full material simultaneously. Because of the discontinuous contact, the tool is set into slight vibration. These tool vibrations cause damage to the final workpiece surface, increasing surface roughness.

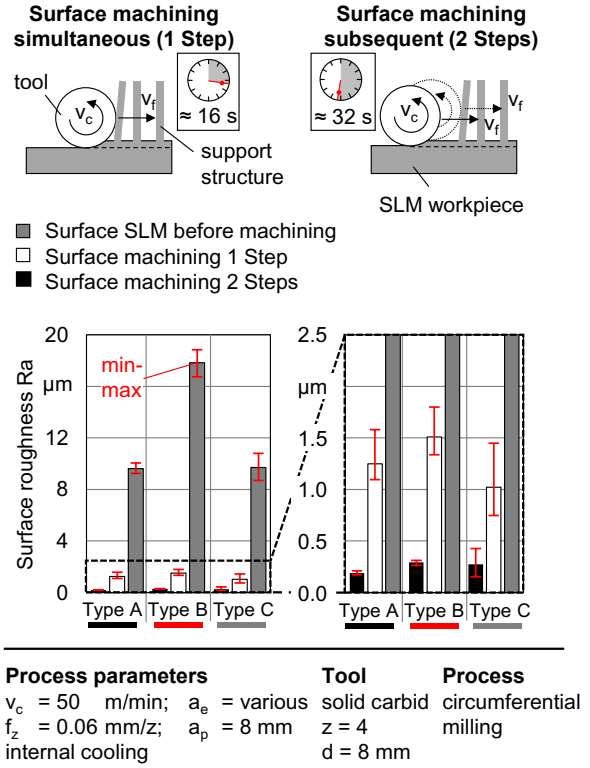

Figure 10 Surface roughness after milling the support structure and milling the SLM component surface for different machining strategies

Theoretically, it is also possible to use higher tooth feed rates in the first step of subsequent machining. Then the machining time would not double compared to simultaneous milling.

4. Conclusion

In the aviation industry, additive manufacturing (AM) is establishing itself as a production technology for aviation components, thus continuously reducing weight and therefore emissions. Because AM parts do not fulfill the quality requirements of finished components after selective laser melting (SLM), precision machining is necessary. In this paper, the following results and conclusions can be obtained for the machining of SLM components:

- Thin-walled functional surfaces present a challenge during machining because they deflect and vibrate during the process.
- Clamping systems, which support the workpieces during milling, significantly improve the machining behavior. This prevents the workpiece from being deflected, resulting in high dimensional accuracy.
- The design of the SLM support structure geometries has a strong impact on the milling behavior. A strong correlation between the material volume fraction and the process forces during milling can be seen.
- By milling, the surface roughness can be strongly reduced compared to the surface of the SLM components after the selective laser melting process step.
- The milling strategy has a high influence on the surface roughness when machining support structures. On the one hand, a high surface quality can be achieved by subsequent machining of the support structure and precision machining (2 steps). On the other hand, with the simultaneous support structure removal and precision machining (1 step) the roughness is higher, but the machining time is reduced.

5. Acknowledgements

The results of this publication have been achieved in the project ALM2AIR funded by the German Federal Ministry for Economic Affairs and Energy under funding code 20W1501M. We would like to thank our industrial partners Airbus, Liebherr Aerospace, Premium AEROTEC and CERATIZIT Balzheim for their collaboration and support.

References

[1] AIRBUS S.A.S.: Global Market Forecast, Cities, Airports & Aircraft 2019-2038. www.airbus.com.

[2] European Comission: EUROPEAN AERONAUTICS: A VISION FOR 2020, Luxembourg, European Union, 2001.

[3] European Commission: Flightpath 2050, Europe's Vision for Aviation. Luxembourg: European Union, 2011.

[4] Emmelmann, C.; Sander, P.; Kranz, J.; Wycisk, E.: Laser Additive Manufacturing and Bionics: Redefining

Lightweight Design. Physics Procedia, Volume 12, Part A, 2011, p. 364-368.

[5] Bendsoe, P.; Sigmund; O.: Topology Optimization: Theory, Methods and Applications. Springer-Verlag, Berlin, Heidelberg, 2003.

[6] Thompson, M. K.; Moroni, G.; Vaneker, T.; Fadel, G.; Campbell, R. I.; Gibson, I.; Bernard, A.; Schulz, J.; Graf, P.; Ahuja, B.; Martina F.: Design for Additive Manufacturing: Trends, opportunities, considerations, and constraints. CIRP Annals, Volume 65, Issue 2, 2016, p. 737-760.

[7] Dumas, M.; Cabanettes, F.; Kaminski, R.; Valiorgue, F.; Picot, E.; Lefebvre, F.; Grosjean, C.; Rech, J.: Influence of the finish cutting operations on the fatigue performance of Ti-6Al-4V parts produced by Selective Laser Melting. Procedia CIRP, Volume 71, 2018, p. 429-434.

[8] Herzog, D.; Seyda, V.; Wycisk, E.; Emmelmann, C.: Additive manufacturing of metals, Acta Materialia, Volume 117, 2016, p. 371-392.

[9] Spranger, F.; Graf, B.; Schuch, M.; Hilgenberg, K.; Rethmeier, M.: Build-up strategies for additive manufacturing of three dimensional Ti-6Al-4V-parts produced by laser metal deposition. Journal of Laser Applications 30, 022001, 2018.

[10] Greitemeier, D.; Palm, F.; Syassen, F.; Melz, T.: Fatigue performance of additive manufactured TiAl6V4 using electron and laser beam melting. International Journal of Fatigue, Volume 94, Part 2, 2017, p. 211-217.

[11] Kasperovich, G; Hausmann, J.: Improvement of fatigue resistance and ductility of TiAl6V4 processed by selective laser melting. Journal of Materials Processing Technology, Volume 220, 2015, p. 202-214.

[12] Vrancken, B.; Thijs, L.; Kruth, J.-P.; Van Humbeeck, J.: Heat treatment of Ti6Al4V produced by Selective Laser Melting: Microstructure and mechanical properties. Journal of Alloys and Compounds, Volume 541, 2012, p. 177-185.

[13] Hintze, W.; Möller, C.; Schötz, R.: Finish Machining of Titanium Components - Challenges of New Process Chains and Recent Alloys. In: von Estorff, O.; Thielecke, F. (Hrsg.): Proceedings of the 6th International Workshop on Aircraft System Technologies (AST 2017), February 21 - 22, 2017, Hamburg, Germany. Berichte aus der Luft- und Raumfahrttechnik, Shaker Verlag, Aachen, 2017, p. 397-407.

[14] Hintze, W.; Schötz, R.; Mehnen, J.; Köttner, L.; Möller, C.: Helical milling of bore holes in Ti6Al4V parts produced by selective laser melting with simultaneous support structure removal, Procedia Manufacturing, Volume 18, 2018, p. 89-96.

[15] Milton, S.; Morandeau, A.; Chalon, F.; Leroy, R.: Influence of Finish Machining on the Surface Integrity of Ti6Al4V Produced by Selective Laser Melting, Procedia CIRP, Volume 45, 2016, p. 127-130.

[16] Sartori, S.; Bordin, A.; Moro, L.; Ghiotti, A.; Bruschi, S.: The Influence of Material Properties on the Tool Crater Wear When Machining Ti6Al4V Produced by Additive Manufacturing Technologies. Procedia CIRP, Volume 46, 2016, p. 587-590.

[17] Calignano F.: Design optimization of supports for overhanging structures in aluminum and titanium alloys by selective laser melting. Materials & Design, Volume 64, 2014, p. 203-213.

[18] Izamshah, R. R. A.; Mo, J. P. T.; Ding, S: Hybrid deflection prediction on machining thin-wall monolithic aerospace components. Journal of Engineering Manufacture, Volume 226, Issue 4, 2012, p. 592-605.

[19] Smith, S.; Dvorak, D.: Tool path strategies for high speed milling aluminium workpieces with thin webs. Mechatronics, Volume 8, Issue 4, 1998, p. 291 – 300.

[20] Smith, S.; Wilhelm, R.; Dutterer, B.; Cherukuri, H.; Goel, G.: Sacrificial structure preforms for thin part machining. CIRP Annals, Volume 61, Issue 1, 2012, p. 379 - 382.

[21] Heigel, J. C.; Phan, T. Q.; Fox, J. C.;. Gnaupel-Herold, T. H.: Experimental Investigation of Residual Stress and its Impact on Machining in Hybrid Additive/Subtractive Manufacturing. Procedia Manufacturing, Volume 26, 2018, p. 929-940.

[22] AIRBUS S.A.S.: Airbus A350 XWB starts its China tour with debut at Zhuhai Airshow, www.airbus.com, 2016.

[23] Concept Laser: Ahead! Topological optmised components in aviation. www.concept-laser.de, 2017.

[24] Bagehorn, S.; Mertens, T.; Greitemeier, D.; Carton, L.; Schoberth, A.: Surface finishing of additive manufactured Ti-6Al-4V - a comparison of electrochemical and mechanical treatments. 6th EUCASS, 2015.

[25] Altintas, Y.; Engin, S.: Generalized Modeling of Mechanics and Dynamics of Milling Cutters. CIRP Annals, Volume 50, Issue 1, 2001, p. 25-30.

[26] Altintas, Y.; Kilic, Z.M.: Generalized dynamic model of metal cutting operations. CIRP Annals, Volume 62, Issue 1, 2013, p 47-50.